ISSN 1027-4510, Journal of Surface Investigation: X-ray, Synchrotron and Neutron Techniques, 2025, Vol. 19, No. 1, pp. 126–133. © Pleiades Publishing, Ltd., 2025.

The Influence of High-Temperature Heat Treatment on the Evolution of Surface Composition of Rapidly Solidified Foils of Al–Mg–Li–Sc–Zr Alloy

I. A. Stoliar[a], *, V. G. Shepelevich[a], I. I. Tashlykova-Bushkevich[b], **, R. Wu[c], and E. Wendler[d]

[a] *Belarusian State University, Minsk, 220050 Belarus*

[b] *Belarusian State University of Informatics and Radioelectronics, Minsk, 220013 Belarus*

[c] *Harbin Engineering University, Harbin, 150001 PR China*

[d] *Friedrich Schiller University, Jena, 07743 Germany*

**e-mail: uyluana@gmail.com*

***e-mail: iya.itb@bsuir.by*

Received August 10, 2024; revised October 20, 2024; accepted October 20, 2024

Abstract—The influence of high-temperature annealing on the composition of surface layers of rapidly solidified Al–Mg–Li–Sc–Zr alloy foils of 1421 grade obtained by centrifugal quenching from the melt has been studied when heated to 380°C in air depending on the holding time. Surface elemental mapping of the foils annealed for 1 h was carried out by scanning electron microscopy with energy dispersive X-ray microanalysis. The depth distribution of lithium after annealing the samples for 1, 2, and 8 h was studied by nuclear reaction analysis. After short-term annealing for 1 h, the formation of a gradient composition with an increased content of the main alloying elements in the surface layers of annealed foils was found. The thickness of the diffusion layer enriched with lithium is about 3.3 μm. In the 0.3-μm-thick near-surface layer, the average lithium concentration is 30 at %. In contrast to the contact surface, the nonmonotonic character of the lithium concentration profiles of the foils near the free surface includes the presence of a sharp maximum at a depth of 0.3 μm: the lithium content increases from 20 at % in the thin surface layer (0.1 μm) up to 40 at %. During the annealing process, with increasing holding time, an intensive mass transfer of lithium atoms to the depth of the foils is observed. The thickness of the diffusion layer increases 4 times.

Keywords: Al–Mg–Li–Sc–Zr alloy, rapid solidification processing, lithium, magnesium, scandium, mapping, scanning electron microscopy, energy-dispersive X-ray microanalysis, nuclear reaction analysis

DOI: 10.1134/S102745102570020X

INTRODUCTION

Resource-saving methods of obtaining materials such as melt spinning technique, centrifugal solidification, and additive technologies [1–3] allow high metal cooling rates to be achieved and are actively used in modern industrial technologies. Rapidly solidified (RS) alloys are successfully manufactured and used both in the original form of foils, tapes, and powders and in a consolidated state in the production of massive parts from powder raw materials [4, 5]. Therefore, while the use of aluminum-lithium alloys based on the Al–Mg–Li alloying system as high-tech materials for aviation and aerospace technology allows increasing the weight efficiency of aircraft due to the unique influence of lithium on the complex of properties of Al–Mg alloys [6–9], interest in these alloys obtained under nonequilibrium conditions is growing [10]. In particular, as a result of high-speed crystallization of melts, it is possible to create aluminum alloys whose level of physical, chemical, and mechanical characteristics is significantly higher in comparison with traditional metallic materials [2] due to the achievement of high melt cooling rates ($\sim 10^6$ K/s). At the same time, the initial structure of rapidly solidified alloys of complex composition is highly nonequilibrium and, at elevated annealing temperatures, there is a problem of degradation of the structure at various levels and, consequently, the properties of materials with holding time. Therefore, for operation at high working temperatures, it is necessary to investigate the stability of the structure and, consequently, the properties of rapidly solidified aluminum materials over a wide temperature range.

The prospects for the synthesis of the multicomponent Al–Mg–Li–Sc–Zr alloy of 1421 grade under high-speed crystallization conditions are determined by the use of the rare earth metal Sc and the transition metal Zr as modifiers to increase thermal stability, as well as strength and corrosion characteristics. The number of works devoted to the influence of nonequi-

librium conditions of ultrafast quenching from the melt on the structural-phase state of alloys of the Al–Mg–Li system [11, 12] is very limited in comparison with studies of the structure and phase transformations in alloys obtained under nonequilibrium conditions using methods of severe plastic deformation and methods of surface treatment with laser radiation [2, 13–16]. However, a comparison of the mechanical properties of these materials after annealing, for example, microhardness, revealed increased thermal stability of rapidly solidified materials [17–20], associated with the structural-phase state of microcrystalline alloys. Previously, we found that high-speed cooling of the liquid phase of alloy 1421 during quenching causes the formation of a supersaturated solid solution of the α-phase of Al, in which an anomalous increase in the solubility of alloying components that are poorly soluble under equilibrium conditions in aluminum is achieved [21]. It was also established that the structure and phase composition of microcrystalline foils of alloy 1421 differ significantly from the equilibrium state of cast coarse-grained samples of the alloy due to the expansion of the temperature-concentration region of the solid solution and the formation of nonequilibrium phases in the process of its decomposition during annealing, including the metastable lithium-containing phase $Al(Mg, Sc, Zr, Li)_x$ [21]. Later, in [22], during high-temperature annealing with a holding time of 1 h, the effect of a multiple increase in the lithium concentration in the near-surface regions of the foils was revealed for the first time. Continuation of the study of the temperature dependence of the surface segregation of lithium in foils showed that, during low-temperature annealing, on the contrary, depletion of lithium in the surface and deep layers of the samples occurs [23]. The obtained results are of scientific and practical interest and demonstrate the relevance of the direction of research on identifying the patterns of structural-phase transformations in rapidly solidified samples of alloy 1421 during high-temperature annealing. In particular, the choice of optimal modes of strengthening heat treatment is important for studying the problem of the negative influence of temperature effects on the physicochemical and mechanical properties of materials in aggressive gas and liquid environments.

The aim of this work is to study the effect of high-temperature annealing on the surface composition of rapidly solidified Al–Mg–Li–Sc–Zr (1421) alloy foils, including the effect of lithium surface segregation as a function of annealing holding time. In this paper, a comprehensive study of segregation processes in rapidly solidified Al–Mg–Li–Sc–Zr alloy was carried out using scanning electron microscopy (SEM) with the use of X-ray spectral analysis (XRMA) in addition to the nondestructive method of instantaneous nuclear reactions (INR) based on the use of a nuclear reaction on protons (p, α) to determine the concentration profiles of lithium in 1421 alloy foils depending on the distance from the sample surface to the analysis area.

EXPERIMENTAL

The objects of the study were foils of Al (5.8 at %), Mg (8.1 at %), Li (0.03 at %), Zr (0.11 at %), Sc alloy grade 1421 obtained by high-speed crystallization from a melt with a crystallization rate of 10^6 K/s [11], when the melt was poured onto the inner surface of a rotating copper cylinder. As a result, samples of rapidly solidified elongated foil with a thickness of 60–80 μm were obtained, for which it was assumed that the contact surface A is the side in contact with the cylinder and the "free" surface B is the reverse side in contact with air. The foils were annealed at 380°C for 1, 2, and 8 h.

Elemental analysis of the air-contacted surface of annealed foils was studied using an FEI Helios Nanolab 650 dual-beam scanning electron microscope (United States) equipped with an energy-dispersive analyzer attachment. The measurements were carried out at an accelerating voltage of 30 kV in the reflected electron mode.

The redistribution of lithium across the foil depth with annealing holding time was studied by the INR method using a nuclear reaction $^7Li(p, \alpha)^4He$ during irradiation of annealed foils with accelerated protons with an energy of 1.4 MeV. The measurements were carried out on a JULIA tandentron accelerator (3 MV) (Jena University Laboratory for Ion Acceleration) with a detector resolution of 15 keV. The detector in the experiments when obtaining spectra was at a scattering angle of $\theta = 170°$. The diameter of the beam incident on the target was 1 mm. Using the SIMNRA program [24], theoretical spectra were calculated, representing the sample in the modeling as a set of layers of a given thickness of $\times 10^{15}$ at/cm^2 and elemental composition. By generating partial spectra of chemical elements, the best agreement between theoretical and experimental spectra was obtained and, consequently, the depth profile of lithium concentration was determined. To interpret the experimental results, the thickness of the model layers was converted into linear dimensions using the method described in [25], for the first time taking into account the oxide-hydroxide layer [26], the thickness of which on the surface of the foils was estimated to be 1 μm. The statistical error in determining the lithium concentration using the INR method ranged from 5 to 15%.

RESULTS AND DISCUSSION

Figure 1a shows a backscattered electron image of a typical surface morphology of the alloy 1421 foil annealed at 380°C for 1 h. Elemental mapping of the surface of annealed foils was carried out using an X-ray energy-dispersive spectrometer. A typical result of energy dispersive X-ray analysis is shown in Fig. 1b.

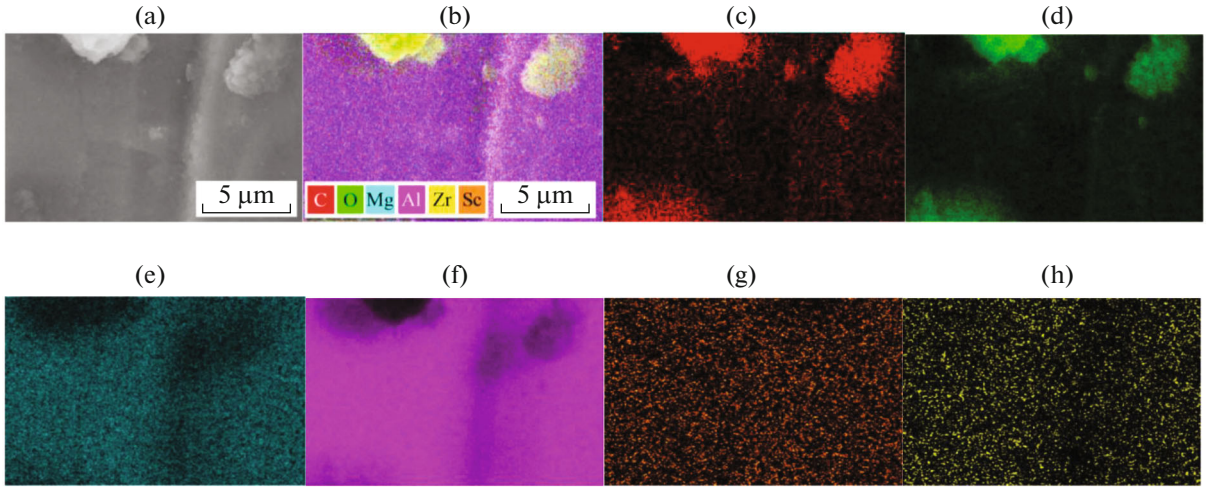

Fig. 1. Image of the air-contacting surface of rapidly solidified 1421 alloy foil annealed at 380°C for 1 h: SEM image obtained in the secondary electron detection mode of a section of foil (a) and the corresponding X-ray microanalysis map of the distribution of the main chemical elements over the surface (b), as well as the distribution of elements obtained in the characteristic X-ray radiation of carbon (c), oxygen (d), magnesium (e), aluminum (f), zirconium (g) and scandium (h) atoms.

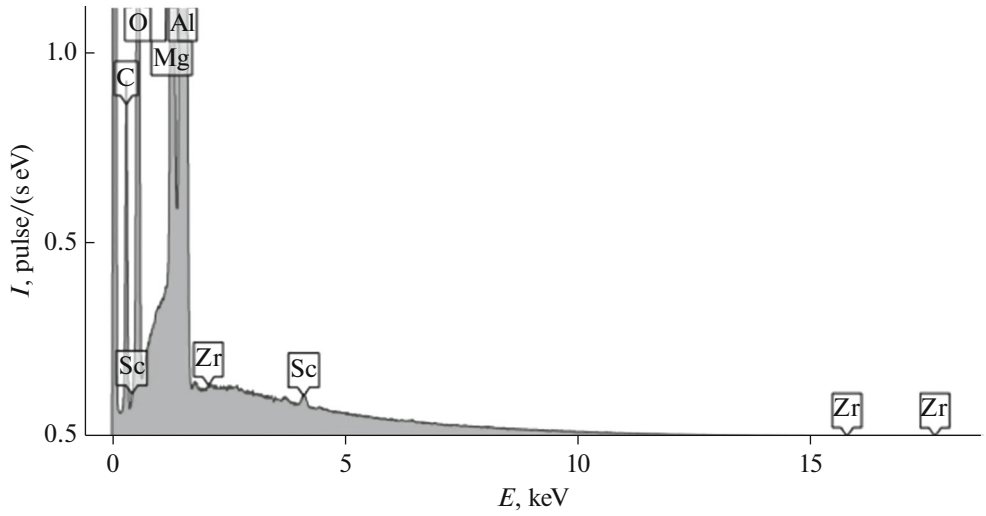

Fig. 2. XRMA spectrum obtained for a section of alloy 1421 foil (an image of which is shown in Fig. 1a) with characteristic lines of chemical elements.

The distribution maps obtained in the characteristic X-ray radiation of carbon, oxygen, magnesium, aluminum, zirconium, and scandium atoms are shown in Figs. 1c–1h, respectively. The change in brightness level values at different points of the map images corresponds to the number of X-ray quanta that hit the detector in a certain energy range. The corresponding energy-dispersive spectrum of the selected section of the foil is shown in Fig. 2. According to the results of X-ray spectral analysis, which does not allow lithium to be recorded, the content of magnesium, scandium and zirconium in the composition of the foil surface is 6.31, 0.14, and 0.03 at %, respectively (Table 1).

Table 1. Results of the study of the chemical composition of the area of the surface of the alloy 1421 foil in contact with air by the X-ray microanalysis method

Elements	Content, at %	Content, wt %
Mg	6.31	5.71
Al	93.52	93.95
Sc	0.14	0.24
Zr	0.03	0.09

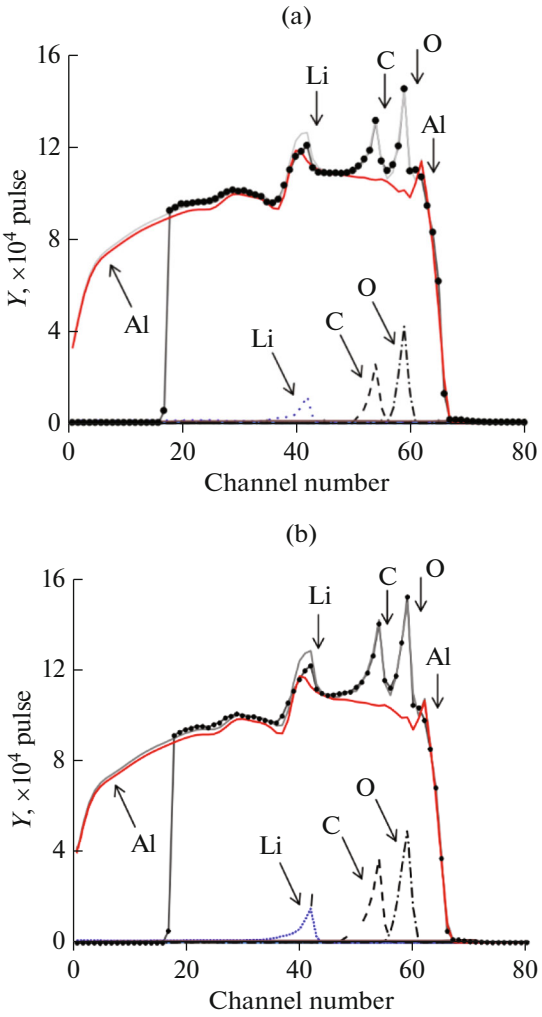

Fig. 3. Experimental spectra (dots) of 1.4 MeV protons backscattered by rapidly solidified 1421 alloy foil annealed at 380°C for 1 h: (a) surface *A* and (b) surface *B*. The solid gray line is the result of modeling in the SIMNRA program. The kinematic boundaries and partial spectra of the Li, C, O, and Al series are shown.

Figures 3 and 4a show typical spectra of backscattered protons and α-particles, products of the nuclear reaction ^{7}Li(p, α)^{4}He, for both surfaces of the alloy Al–Mg–Li–Sc–Zr foil, respectively, after annealing at 380°C for 1 h. Figures 3a and 3b show the experimental proton backscattering spectra, the modeling of which was carried out in the SIMNRA program. Satisfactory agreement between the simulated spectra and the experimental ones was achieved in the entire energy range. The figures also show partial spectra of the main elements, the kinematic boundaries of which are marked by vertical arrows. A comparison of the spectra in Figs. 3a and 3b clearly demonstrates that the content of lithium, carbon, and oxygen is highest in the near-surface layers of the foil surface in contact with air. The magnesium content cannot be determined using SIMNRA modeling because magnesium and aluminum are neighboring elements in terms of atomic number. It is also not possible to model the signals of the alloying elements scandium and zirconium in the high-energy part of the proton backscattering spectra due to the low concentration of these elements in alloy 1421. The α-particle spectra for both surfaces of the 1421 alloy foils annealed at 380°C for 2 and 8 h are shown in Figs. 4b and 4c.

By modeling the experimental spectra, the depth concentration profiles of lithium distribution were obtained (Fig. 5); the layer thickness here and below is indicated in at/cm^2. As previously established, in foils of alloy 1421 after quenching, lithium is distributed uniformly in depth and its content is 9 at % [21]. After one h of annealing at 380°C, the behavior of lithium in the area of both foil surfaces changes. Additional layer-by-layer modeling of the carbon and oxygen distribution made it possible to refine the modeling data for the concentration profiles of lithium atoms. It was found that a diffusion layer enriched with lithium is formed on both surfaces of the foils during annealing and has a thickness of 20 × 10^{18} at/cm^2 (3.3 μm). In the surface layer with a thickness of 3 × 10^{18} at/cm^2 (0.3 μm)

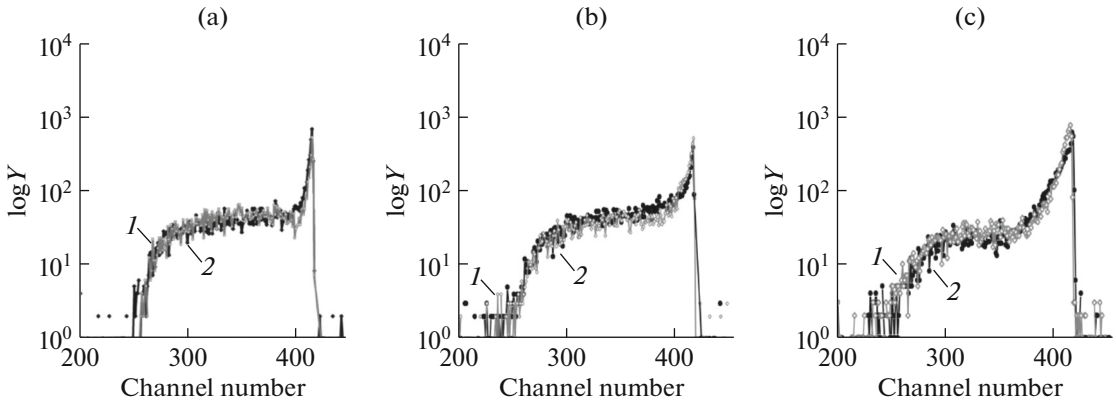

Fig. 4. Experimental spectra of α-particles from the reaction ^{7}Li(p, α)^{4}He for surfaces *A* (*1*) and *B* (*2*) of the alloy 1421 foil annealed at 380°C for 1 (a); 2 (b); and 8 h (c).

on both sides of the annealed foil the average lithium concentration is the same and is 30 at %. Lithium content in the specified layer near the surface *A* is almost constant. At the same time, at the boundary of this layer, near the surface *B*, a local maximum in lithium concentration is observed. It was shown that the lithium content equal to 20 at % in the surface layer of 10^{18} at/cm^2 (0.1 μm) sharply increases to 39 at % with distance from the surface *B*. After annealing the samples for 2 h, the opposite trend was observed: the degree of surface enrichment *A* with lithium increases, unlike the surface *B*. Lithium content in a thin surface layer of 10^{18} at/cm^2 (0.1 μm) of the contact side increases by ~30% and reaches 40 at %. Depth profile of lithium concentration (in a layer of thickness 20 × 10^{18} at/cm^2, 3.3 μm) is characterized by a slower decrease in the Li content with depth in the sample than that after short-term annealing for 1 h. At the same time, on the opposite side *B*, near which the largest lithium concentration gradient occurs after annealing for 1 and 2 h, the maximum lithium content is 28 at % at a depth of 10^{18} at/cm^2 (0.1 μm). In the next layer, at a depth of 0.1–0.3 μm, the lithium concentration decreases almost twofold, to 15 at %. Note that near the surface *A* the lithium-rich layer is wider: the Li concentration decreases slowly with depth in a layer of thickness 20 × 10^{18} at/cm^2 (3.3 μm). With an increase in the isothermal annealing time to 8 h, firstly, a tendency for the lithium content in the surface layers to equalize to a depth of 3 × 10^{18} at/cm^2 (0.3 μm) is detected: on both sides of the foils, within the accuracy of the INR method, the lithium concentration reaches 30 at %. Secondly, the thickness of the surface layer with the nonuniform distribution of lithium in depth increases to 30 × 10^{18} at/cm^2 (5 μm). Concentration gradient of lithium near the surface *A* is higher compared to the surface *B*. It should be noted that the lithium concentration in the layer deeper than 30 × 10^{18} at/cm^2 (5 μm) remains virtually unchanged, reaching a minimum value of 4 at %, which is 56% lower than that of unannealed samples.

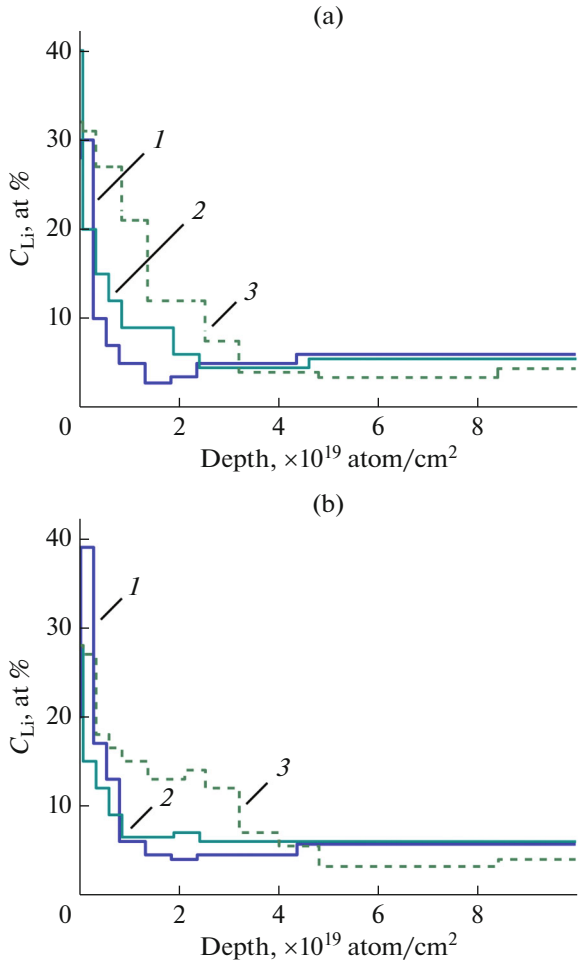

Fig. 5. Depth distribution of lithium atoms *C* in the area of surfaces *A* (a) and *B* (b) of alloy 1421 foils annealed at 380°C for 1 (*1*); 2 (*2*); and 8 h (*3*).

As is known, the operational characteristics of industrial alloys include such properties as heat resistance, wear resistance, cold resistance, and antifriction. Additionally, in practice, the physicochemical properties of the surface layers of materials containing surface-active elements are important, among which are oxidation and corrosion resistance, as well as mechanical properties such as hardness, strength, plasticity, etc. [7, 8]. It should be noted that in the case of nonequilibrium crystallization, alloys are formed that are characterized by a composition gradient, when the concentration of alloying elements and impurities changes with distance from the surface [27, 28]. One of the characteristic features of such morphology is that as a result of the evolution of the composition of the surface layers during heat treatment, the properties of the materials will also change. However, in alloys of the Al–Mg–Li system the behavior patterns of lithium in the annealing process have not been sufficiently studied due to the limitations of a number of traditional methods, such as X-ray spectral analysis, when profiling light elements over the depth of alloys, as well as the inconsistency of known experimental results, such as in [29–31], due to the insufficient accuracy of indirect methods based on measuring microhardness or electrical resistance.

At the same time, the maximum strengthening of alloys of the Al–Mg–Li system is achieved by high-temperature annealing. Therefore, modern research aimed at developing high-strength Al–Li-based alloys using Sc/Zr or Er/Zr microalloying and studying the stability of their structure, phase composition and, consequently, properties after annealing are of considerable interest and practical importance. As a result of microalloying in Al–Li alloys a core–shell phase with a face-centered cubic lattice of the structural type $L1_2$ is formed based on Al_3(Li, Sc, Zr) or Al_3(Li, Er, Zr) compounds [32, 33]. This phase exists in two forms: a

primary phase, which has the effect of reducing the grain size of the matrix structure of Al–Li alloys, and a metastable phase, which is released as nanoparticles during the subsequent annealing process, is coherent with the solid solution of the α-phase of Al, and provides the greatest effect of alloy strengthening during heat treatment. It is noted that coherence with the matrix of selections with the structure of the type $L1_2$ depends on temperature and improves after alloying with Mg. The problem with the use of traditional casting is the fact that the particles of the primary phases formed in the cast Al–Li and Al–Mg–Li alloys are relatively large in size and have a negative effect on the strength and toughness of the alloys [34]. These relatively large particles of the primary phase not only worsen the corrosion characteristics and mechanical properties of the alloy but also weaken the possibilities of dispersion strengthening by secondary phase nanoparticles during subsequent annealing [34, 35], since phases with a structure of the type $L1_2$, containing rare earth elements, tend to precipitate at high temperatures. Consequently, for strengthening alloys by creating core-shell nanoparticles during subsequent annealing, high-speed crystallization methods are of scientific and practical interest, allowing one to exceed the melt cooling rate of about 100 K/s, which is typical for most methods of obtaining microcrystalline alloys, and to synthesize materials characterized by a higher degree of homogeneity and uniformity (phase and structural), expanding the scope of application of the used and newly developed alloy compositions.

The important role of crystal lattice defects (primarily vacancies and dislocations) in diffusion processes during annealing, leading to structural transformations in aluminum alloys synthesized under nonequilibrium conditions, is known. In particular, crystal lattice defects reduce the activation energy of surface diffusion and facilitate its occurrence. It has been shown that with ultrafast quenching from the melt, the effect of "freezing" defects, for example, excess vacancies, can be achieved [36]. However, the analysis of annealing experiments is complicated by the following structural factors. On the one hand, the presence of atoms of alloying elements (impurities) affects the formation and migration of defects in aluminum. In particular, impurity atoms can contribute to either an increase or a decrease in the concentration of vacancies. On the other hand, difficulties arise because the interaction of defects of different types affects both the energy of their formation and the activation energy of movement. Based on the experimental data obtained in this work, it can be concluded that the discovered fact of enrichment of the surface of foils of the Al–Mg–Li alloy system containing scandium and zirconium with lithium after annealing for 1 h is explained by the formation of a nonequilibrium structure of the material as a result of high-speed crystallization, which changes the kinetics of the decomposition of the supersaturated solution and strongly influences the processes of phase transformations along with the diffusion redistribution of alloying elements during annealing of rapidly solidified samples. At the annealing stages of rapidly solidified alloy 1421 in the temperature range of 280–450°C, processes occur in the foils that lead to an intensive increase in the specific volume and particle size of the following metastable lithium-containing phases: Al_2MgLi (S_1-phase) and phases of variable composition $Al(Mg, Sc, Zr, Li)_x$ [21]. The increased lithium content on the free surface of the 1421 alloy foils annealed at 380°C may be due to the comparatively finer grains of the material near the surface *B* and, consequently, the formation of a high proportion of grain boundaries in the sample volume. It was found that increasing the duration of high-temperature annealing stimulates the process of lithium heterodiffusion, as evidenced by the increase in its concentration at depth in the sample (Fig. 5).

Thus, in order to establish the influence of structure formation processes in phase transformations during annealing of rapidly solidified lithium-containing aluminum alloys on high-temperature mechanical properties and corrosion behavior, it is necessary to continue research and identify the conditions for the release and decomposition of metastable strengthening nanoparticles with a core-shell structure during heat treatment. The development of resource-saving technologies for the synthesis of Al–Mg–Li alloys and the production of semifinished products from them using centrifugal quenching from the melt requires solving a number of applied and fundamental problems related to the study of the relationship between the processes of formation of phases of intermetallic compounds and surface segregation of alloying elements. The development of temperature-time processing modes will allow optimizing the physical, chemical, and mechanical properties and increasing the resource characteristics of multicomponent alloys of the Al–Mg–Li system for such knowledge-intensive industries as powder metallurgy, mechanical engineering, instrument making, and enterprises creating aviation and rocket and space technology.

CONCLUSIONS

Thermal stability of the structure of rapidly solidified foils of multicomponent alloy 1421 were studied after annealing in open air at 380°C for 1, 2, and 8 h. Using the elemental mapping of foils, a tendency for the content of magnesium and scandium to increase on the surface of the samples after annealing for 1 h was detected. Their surface concentration, measured on the "free" side of the foils, increases by 9 and 27%, respectively, compared to the calculated content in the alloy. The concentration of zirconium remains unchanged within the measurement error. A nonmonotonic type of spatially inhomogeneous distribution of lithium in the surface layers of annealed foils

was established, characterized by the presence of sharp maxima near the surface of the sample on the experimentally measured concentration profiles of lithium after annealing. The peak lithium concentration in a thin 0.3 μm thick surface layer on the "free" side of the annealed foil reaches 40 at %, which is 1.3 times higher than that near the contact side of the foil. With an increase in the annealing time to 8 h, the thickness of the lithium-enriched surface layer increases fourfold. A more intense diffusion of lithium into the depth of the foils was detected in the area of the contact surface.

FUNDING

I.I. Tashlykova-Bushkevich expresses her gratitude to the Ministry of Education of the Republic of Belarus for a travel grant allocated for an internship at the Friedrich Schiller University (November 22, 2019–December 5, 2019, Jena, Germany).

CONFLICT OF INTEREST

The authors of this work declare that they have no conflicts of interest.

REFERENCES

1. T. Pinomaa, A. Laukkanen, and N. Provatas, MRS Bull. **45** (11), 910 (2020). https://doi.org/10.1557/mrs.2020.274
2. W. Kurz, M. Rappaz, and R. Trivedi, Int. Mater. Rev. **66** (1), 30 (2020). https://doi.org/10.1080/09506608.2020.1757894
3. Y. Gu, X. He, and D. Han, Comput. Mater. Sci. **199**, 110812 (2021). https://doi.org/10.1016/j.commatsci.2021.110812
4. K. Tsaknopoulos, C. Walde, Jr. V. Champagne, and D. Cote, JOM **71** (1), 435 (2019). https://doi.org/10.1016/j.msea.2018.09.017
5. A. G. Malikov, A. A. Golyshev, and I. E. Vitoshkin, Prikl. Mekh. Tekh. Fiz. **64** (1), 36 (2023). https://doi.org/10.15372/PMTF202215159
6. Y. Wang, Z. Zhang, R. Wu, J. Sun, Y. Jiao, L. Hou, J. Zhang, X. Li, and M. Zhang, Mater. Sci. Eng. A **745** (1), 411 (2019). https://doi.org/10.1016/J.MSEA.2019.01.011
7. A. Yu. Andryushkin, O. O. Galinskaya, and A. B. Sigaev, Balt. Gos. Tekh. Univ., (2015).
8. V. V. Antipov, N. I. Kolobnev, and L. B. Khokhlatova, Aviats. Mater. Tekhnol., No. 5, 183 (2012).
9. B. V. Ovsyannikov, Tekhnol. Legk. Splavov, No. **1**, 97 (2014).
10. Q. Kuang, R. Wang, C. Peng, and Z. Cai, J. Alloys Compd. **883**, 160937 (2021). https://doi.org/10.1016/j.jallcom.2021.160937
11. T. Gancarz, A. Dobosz, P. Bogno, G. Cempura, N. Schell, R. Chulist, and H. Henein, Mater. Charact. **178**, 111290 (2021). https://doi.org/10.1016/j.matchar.2021.111290
12. M. G. Stepanova, V. I. Valyaeva, N. S. Gerchikova, and N. A. Parkhomenko, Vseross. Nauchno-Issled. Inst. Aviats. Mater., No. 7, 22 (1983).
13. I. G. Brodova, A. N. Petrova, and I. G. Shirinkina, Izv. Ross. Akad. Nauk, Ser. Fiz. **76** (11), 1378 (2012).
14. M. Furukawa, P. B. Berbon, T. G. Langdon, Z. Horita, M. Nemoto, N. K. Tsenev, and R. Z. Valiev, Metall. Mater. Trans. A **29**, 169 (1998). https://doi.org/10.1007/s11661-998-0170-6
15. L. I. Kaigorodova, D. Yu. Rasposienko, V. G. Pushin, V. P. Pilyugin, and S. V. Smirnov, Fiz. Met. Metalloved. **120** (2), 169 (2019).
16. A. Malikov, A. Orishich, N. Bulina, E. Karpov, and M. Sharafutdinov, Mater. Sci. Eng. A **765**, 138302 (2019). https://doi.org/10.1016/j.msea.2019.138302
17. P. A. Sivtsova and V. G. Shepelevich, in *Proceedings of the 7th All-Russian Scientific and Technical Conference with International Participation* (Moscow, 2008), p. 10.
18. V. G. Shepelevich, Vestn. Beloruss. Gos. Univ., Ser. 1:Fiz., Mat., Mekh., No. 2, 13 (2014).
19. N. K. Tsenev, V. N. Perevezentsev, M. Yu. Shcherban', and A. N. Tsenev, Zh. Tekh. Fiz. **80** (6), 68 (2010).
20. A. V. Nokhrin, Ya. S. Shadrina, V. N. Chuvil'deev, V. I. Kopylov, A. A. Bobrov, and K. V. Likhnitskii, Poverkhn.:Rentgenovskie, Sinkhrotronnye Neitr. Issled., No. 1, 24 (2022).
21. V. G. Shepelevich, I. A. Bushkevich, E. Vendler, and I. I. Tashlykova-Bushkevich, Poverkhn.: Rentgenovskie, Sinkhrotronnye Neitr. Issled., No. 6, **101** (2019). https://doi.org/10.1134/S020735281906012X
22. I. A. Stolyar, V. G. Shepelevich, E. Wendler, and I. I. Tashlykova-Bushkevich, Poverkhn.:Rentgenovskie, Sinkhrotronnye Neitr. Issled., No. 7, **96** (2021). https://doi.org/10.31857/S1028096021070190
23. I. A. Stolyar, V. G. Shepelevich, I. I. Tashlykova-Bushkevich, and E. Wendler, Poverkhn.:Rentgenovskie, Sinkhrotronnye Neitr. Issled., No. 2, **23** (2023). https://doi.org/10.31857/S1028096023020139
24. M. Mayer, *SIMNRA, a Simulation Program for the Analysis of NRA, RBS and ERDA* (Am. Inst. of Phys., New York, 1999).
25. A. F. Gurbich, Nucl. Instrum. Methods Phys. Res., Sect. B **268**, 1703 (2010). https://doi.org/10.1016/j.nimb.2010.02.011
26. I. I. Tashlykova-Bushkevich, V. G. Shepelevich, I. A. Stolyar, A. V. Romanchuk, and A. R. Yaps, in *Proceedings of the XVII International Scientific and Technical Conference* (Moscow, 2020), p. 40.
27. G. A. Vershinin, Mezhdunar. Nauchno-Issled. Zh. **8–2** (39), 95 (2015).
28. I. I. Tashlykova-Bushkevich, Yu. S. Yakovenko, V. G. Shepelevich, and I. S. Tashlykov, Fiz. Khim. Obrab. Mater., No. 3, 65 (2016).

29. T. Schoeberl and S. Kumar, J. Alloy Compd. **255**, 135 (1997). https://doi.org/10.1016/S0925-8388(96)02818-6

30. K. K. Soni, D. B. Williams, D. E. Newbury, G. Gillen, P. Chi, and D. S. Bright, Metall. Mater. Trans. A **24**, 2279 (1993). https://doi.org/10.1007/BF02648601

31. J.-P. Harvey, S. Singh, K. Oishi, B. Acheson, R. Turcotte, D. Pilon, J. Lavoie, and B. Gange, Mater. Des. **198**, 109293 (2021). https://doi.org/10.1016/j.matdes.2020.109293

32. V. I. Elagin, V. V. Zakharov, S. G. Pavlenko, and T. D. Rostova, Fiz. Met. Metalloved. **60**, 97 (1985).

33. C. B. Fuller and D. N. Seidman, Acta Mater. **53**, 5415 (2005). https://doi.org/10.1016/j.actamat.2005.08.015

34. Y. Wang, S. Zhang, R. Wu, N. Turakhodjaev, L. Hou, J. Zhang, S. and Betsofen, J. Mater. Sci. Technol. **61**, 197 (2021). https://doi.org/10.1016/j.jmst.2020.05.061

35. Y. Zhu, M. Zhou, Y. Geng, S. Zhang, T. Xin, G. Chen, Y. Zhou, X. Zhou, R. Wu, and Q. Shi, J. Mater. Sci. Technol. **184**, 245 (2024). https://doi.org/10.1016/j.jmst.2023.10.019

36. I. Ya. Dekhtyar, Usp. Fiz. Nauk **62**, 99 (1957).